



# Shipborne Wind Measurement and Motion-induced Error Correction by Coherent Doppler Lidar over Yellow Sea in 2014

Xiaochun. Zhai<sup>1</sup>, Songhua. Wu<sup>1,2</sup>, Bingyi. Liu<sup>1,2</sup>, Xiaoquan. Song<sup>1,2</sup>, Jiaping. Yin<sup>3</sup>

<sup>1</sup>Ocean Remote Sensing Institute, Ocean University of China, Qingdao, 266100, China

5 <sup>2</sup>Laboratory for Regional Oceanography and Numerical Modelling, Qingdao National Laboratory for Marine Science and Technology, Qingdao, 266100, China

<sup>3</sup>Seaglet Environmental Technology, Qingdao, 266100, China

Correspondence to: S. Wu ([wush@ouc.edu.cn](mailto:wush@ouc.edu.cn))

**Abstract.** Shipborne wind observations by the Coherent Doppler Lidar (CDL) have been conducted to study the structure of the Marine Atmospheric Boundary Layer (MABL) during the 2014 Yellow Sea campaign. This paper evaluates uncertainties associated with the ship motion and presents the correction methodology regarding lidar velocity measurement based on modified 4-Doppler Beam Swing (DBS) solution. The errors of calibrated measurement, both for the anchored and the cruising shipborne observations, are comparable to those of ground-based measurements. The comparison between the lidar and radiosonde gives the bias  $-0.1 \text{ ms}^{-1}$  and the standard deviation  $0.75 \text{ ms}^{-1}$  for the wind speed measurement, and shows the bias  $2.8^\circ$  and the standard deviation  $9.81^\circ$  for the wind direction measurement. The biases and random errors of horizontal wind speed are also estimated using the error propagation theory and frequency spectrum analysis, respectively. The results show that the biases are mainly related to the measuring error of the ship velocity, and lidar pointing error and the random errors are mainly determined by the Signal-to-Noise Ratio (SNR) of lidar backscattering spectral signal. It allows for the retrieval of vertical wind, based on one measurement, with random error below  $0.15 \text{ ms}^{-1}$  for appropriate SNR threshold and bias below  $0.02 \text{ ms}^{-1}$ . The combination of the CDL attitude correction system and the accurate motion correction process has the potential of continuous long-term high temporal and spatial resolution measurement for MABL thermodynamic and turbulence process.

## 1 Introduction

The vertical structure of atmospheric variables in the Marine Atmospheric Boundary Layer (MABL) plays an important role in the earth's climate system, governing exchanges of energy, sensible heat, water vapour and momentum between ocean and the overlying atmosphere (Rocers et al., 1995; Wulfmeyer and Janjic, 2005), and the turbulence characteristics are significant for understanding the driving and coupling mechanisms and for parameterizing ocean-atmosphere interaction process. There are many studies on the turbulent fluxes measurement over the sea surface (Axford, 1968; Mitsuta et al., 1974; Bradley et al., 1991; Fujitani, 1992; Hawley et al., 1993; Shao, 1995; Tsukamoto et al., 1995; Song et al., 1996; Edson et al., 1998; Miller et



al., 2008). One of the most direct techniques for measuring surface fluxes is eddy-correlation, which utilizes the covariance of mixing ratios and vertical wind velocity (Lenschow et al., 1981; Ancil et al., 1994; Fairaill et al., 2000), but the wind velocity is complicated by the contamination due to platform motion, representing a major source of uncertainty in measurement of turbulence and air-sea interaction. Several techniques have been used to correct the wind vector measured at sea for the efforts of platform motion (Fujitani, 1992; Dunckel et al., 1974; Song et al., 1996; Edson et al., 1998; Schulz et al., 2005). Fujitani (1985) used a Stable Platform System (SPS) consisting of a vertical gyro-stabilized system and three accelerometers to measure the turbulent flux on the ship, and concluded that this system was applicable to measurement under the rough sea surface condition. A similar method was also used on a buoy (Ancil et al., 1994). This gyro-stabilized system can provide roll, pitch and yaw angles describing the ship's orientation in a fixed frame, which can be used directly in the total rotational coordinate transformation matrix. Song et al (1996) used a Strapped-Down System (SDS) consisting of six accelerometers to measure the air-sea fluxes in the Western Tropical Pacific and estimated that the system appeared to be relatively robust for use at sea for extended period. In SDS, the attitude angles should be calculated indirectly from the strapped-down angular rate sensors. Edson (1998) also used the SDS consisting of three orthogonal angle rate sensors and three orthogonal linear accelerometers to compute direct covariance fluxes from anemometers mounted on a moving platform at sea, and found that the results were in good agreement with fluxes derived using the bulk aerodynamic method. Miller et al (2008) modified E98 procedure to explicitly account for misalignment between anemometers and motion sensors.

The Coherent Doppler Lidars (CDL) have proven to be powerful tools with high temporal and spatial resolution, providing nearly continuous particle backscatter, wind profile observation in the clear atmosphere, which is vital for the vertical structure of turbulent characteristics measurement in MABL. Unlike the conventional in-situ wind measuring methods, CDL can only detect the line-of-sight (LOS) velocity which is the projection of the horizontal and vertical velocity along the laser beam direction, thus it is necessary to conduct measurement at three or more different directions of the probing beam to retrieve the wind velocity (Werner 2005; Cheong et al., 2008). More complicated attitude correction should be considered when CDL is carried out at a moving platform such as ship or aircraft since the orientation of transmitting laser beam is not fixed and the speed of the ship itself and ocean wave will be stacked to the LOS velocity, which has more obvious effect on vertical velocity. Several researches have been carried out to study the CDL platform motion correction either by actively stabilizing the instrument based on robust mechanical compensation system or by accurately measuring platform motion and correcting for this after the fact. Wolfe et al (2007) and Pichugina et al (2012) deployed the NOAA High Resolution Doppler Lidar (HSRL) along with the first use of a motion compensation system at sea in 2004. The HSRL control computer can drive the scanner to actively stabilize the pointing of the scanner and modified Velocity Azimuth Display (VAD) technique are used in the mean-profile calculation. Hill et al (2005; 2008) used the NOAA HSRL with a SDS to compensate for the orientation of the lidar's scanning unit for the ship's motion and concluded that the attitude correction depends on the velocity of the seatainer and on the motion of the hemispheric scanner relative to the seatainer. Wulfmeyer et al (2005) corrected the vertical velocity using LOS velocity in zenith stare mode and horizontal wind derived from VAD mode using NOAA HSRL. Lacking real-time



control of the scanning head orientation, Achtert et al (2015) placed the CDL instrument on a motion-stabilization platform to remove the effect of ship motion, and the five-point geometrical wind solution and the four-point sinusoidal fit method were used to obtain wind profiles, showing that motion stabilization was successful for high wind speed in open water and the resulting wave condition. Reitebuch et al (2001) presented the instrumental correction required for the vertical wind retrieval from an airborne CDL using conical scanning pattern measurement and recalculation of the lidar mounting angle based on the ground return speed and distance. It can be seen that actively mechanical compensation system is used in most of these studies. Especially, the improvements in technology along with decreasing costs and robust correction process are increasing needed. In order to simplify the mechanical structure and to easily install the CDL on the ship platform, our study did not use any active stabilization method. Instead, we only use a relative simple but robust algorithm to achieve the motion correction. This method is very easy to use in limited space under the conditions of the shipborne measurements.

With this method, we carried out the first cruise campaign. In order to measure the wind field and turbulence characteristics of MABL over the Yellow Sea, the experimental investigation was undertaken by *Dongfanghong-2* research vessel affiliated with Ocean University of China in 2014. The Yellow Sea, a marginal sea of the Pacific Ocean, is the northern part of the East China Sea. It is located between mainland China and the Korean Peninsula. Few studies have been devoted to measure the boundary layer dynamics in this region. This paper gives a thorough analysis of the attitude correction for lidar velocity measurement. To illustrate the effect of ship motion on Doppler measurement, we focus on horizontal and vertical wind profile analysis. In Sect. 2, the specifications of CDL and especially its attitude correction system are described in detail, and the velocity correction method is also discussed in Sect. 2. In Sect. 3, the corrected results of horizontal wind are analysed and compared with simultaneous radiosonde data. A case study is presented to analyse the effect of the ship velocity and horizontal wind on vertical velocity. Furthermore, the error analysis of horizontal and vertical velocity is also specifically analysed in Sect. 3. Finally, Sect. 4 provides a summary and concluding remark.

## 2 Lidar technology and methodology

The CDL system WindPrint S4000, manufactured by Seaglet Environmental Technology, is based on all-fibre laser technology and the heterodyne detection technology. Wu et al (2016) and Zhai et al (2017) have given a comprehensive description of CDL. The lidar has a semi-conductor single frequency seed laser that provides both the local oscillator reference beam for heterodyne detection as well as the transmitted beam. The laser operates at a wavelength of 1.55  $\mu\text{m}$  with a linewidth (full width at half maximum from Lorentzian) of 1.6 kHz. Using the Acoustic Optic Modulator (AOM) and Master Oscillator Power-Amplifier (MOPA) configuration, achieved pulsed energy is approximately 150  $\mu\text{J}$  with a pulse repetition frequency of 10 kHz. The pulse width produced by the modulation is adjustable from 100 ns to 400 ns, thus the spatial resolution can be varied from 15 m to 60 m. We typically operate CDL with a pulse width of 200 ns in this paper. The transmitted beam is directed into the atmosphere using the 3D scanner that contains azimuth mirror and elevation mirror. The scanner allows the



lidar beam to probe the hemisphere above the container by means of the “azimuth rotation” and “elevation rotation”. The detection range of 4000 m (maximum 6000 m at a proper aerosol concentration) enables the system to monitor the complete MABL structure most of the time. A fibre optical circulator and a telescope are used as the optical transceiver. The atmospheric return beam passes through the 3D hemispheric scanner and the optical transceiver, and is combines with the local oscillator reference beam at the balanced detector. Using heterodyne detection, the frequency difference between the atmospheric return beam and the local oscillator reference beam is detected, which is the measured Doppler shift caused by the relative motion of atmospheric scatters and the lidar system. The real-time analysis based on Fast Fourier Transform (FFT) is used with a Field Programmable Gate Array (FPGA) signal processor. Table 1 lists the general specifications of CDL.

Figure 1 shows the CDL setup on Dongfanghong-2 research vessel during the MABL field project over Yellow Sea in 2014. The scanner is mounted on the roof of the cabinet container with two fixed Global Navigation Satellite System (GNSS) antennas. Generally, the attitude correction system uses GNSS to define the Earth coordinate system, where the ship speed, heading angle and earth location including the longitude and latitude in Earth coordinate system can be obtained. Another important part of attitude correction system is the inertial navigation system. The inertial navigation system is rigidly mounted on the base of the scanner, instead of the deck of the ship, to keep constant relative angles with reference to the transmitting laser beam. It records the lidar motion angles including pitch, roll, laser beam azimuth and elevation, thus the recorded information is the exact lidar itself attitude in lidar coordinate system. After installation, a hard target calibration is firstly performed to determine the initial orientation of the laser beam in the Earth coordinate system, then the standard ship attitude definition can be determined based on the relationship between the lidar and the ship coordinate system, which will be used in the following ship motion correction process. It can be seen that there exists no laser direction error determined by misalignment between the ship and laser beam axis.

Ship motion turns out to be an important error source for the determination of turbulence variables using shipborne CDL (Wulfmeyer and Janjic, 2005). To study boundary layer dynamics, the atmospheric wind velocity in Earth coordinate system is required, so the compensation for the pointing error and along-beam platform velocity due to ship motion need to be determined using attitude correction system.

As can be seen in Fig. 2, the ship coordinate system ( $X_s - Z_s$ ) is defined as  $X_s$  axis along centre line of ship, positive toward bow,  $Y_s$  axis is perpendicular to  $X_s$ , and positive toward starboard,  $Z_s$  axis is positive toward the bottom. The attitude of the ship can be expressed by roll  $\varphi$ , pitch  $\theta$  and heading angles  $\psi$ . The  $\varphi$ ,  $\theta$  and  $\psi$  refer to rotations about  $X_s$ ,  $Y_s$ , and  $Z_s$  axes, respectively. Specifically, positive  $\varphi$  is defined when the port is up, and positive  $\theta$  is defined when the bow is up. The  $\psi$  is defined  $0^\circ$  when the bow points to north in Earth coordination system. The Earth coordinate system ( $X_g - Y_g - Z_g$ ) is defined as  $X_g$  axis along north-south direction, positive toward to north,  $Y_g$  axis is along east-west direction, and positive toward to east,  $Z_g$  axis is positive toward the bottom.



In the ship coordinate system, the recorded azimuth and elevation of the transmitting laser are  $\varphi_s$  and  $\theta_s$ , respectively.  $\varphi_s$  is defined as the angle between the projection of transmitting laser path on  $X_s - Y_s$  plane and the positive  $X_s$  axis. When looking downw,  $\varphi_s$  increases in a clockwise direction.  $\theta_s$  is defined as the angle between the transmitting laser path and the  $X_s - Y_s$  plane. Therefore, the direction of the transmitting laser in the ship coordinate system can be expressed by a unit vector

5  $\vec{r}_s$  as (Hill, 2005; Liu et al., 2010).

$$\vec{r}_s = \begin{pmatrix} x_s \\ y_s \\ z_s \end{pmatrix} = \begin{pmatrix} \cos \theta_s \cos \varphi_s \\ \cos \theta_s \sin \varphi_s \\ -\sin \theta_s \end{pmatrix} \quad (1)$$

The coordinate transformation from the ship coordinate system to that of the Earth is needed. According to the transformation matrix from the product of three rotation matrixes shown in Eq. (2), the unit vector  $\vec{r}_g$  of transmitting laser direction in Earth coordinate system can be expressed as Eq. (3)

$$H_2 = \begin{pmatrix} \cos \theta & 0 & -\sin \theta \\ 0 & 1 & 0 \\ \sin \theta & 0 & \cos \theta \end{pmatrix}, H_3 = \begin{pmatrix} \cos \psi & \sin \psi & 0 \\ -\sin \psi & \cos \psi & 0 \\ 0 & 0 & 1 \end{pmatrix}, H_1 = \begin{pmatrix} 1 & 0 & 0 \\ 0 & \cos \varphi & \sin \varphi \\ 0 & -\sin \varphi & \cos \varphi \end{pmatrix}, \quad (2)$$

$$\vec{r}_g = \begin{pmatrix} x_g \\ y_g \\ z_g \end{pmatrix} = (H_1 H_2 H_3)^{-1} \vec{r}_s \quad (3)$$

Where  $H_1$ ,  $H_2$ ,  $H_3$  are the rotation matrices of roll, pitch and heading, respectively (Hill, 2005).

10 Once the unit vector  $\vec{r}_g$  is calculated from Eq. (2)-(3), the azimuth  $\varphi_g$  and elevation  $\theta_g$  of LOS observation in Earth coordinate system can be calculated

$$\varphi_g = \arctan(y / x) \quad (4)$$

$$\theta_g = -\arcsin z \quad (5)$$

For a shipborne CDL, the recorded velocity corresponds to the relative velocity along the laser beam direction between the ship and the atmospheric target, where the ship platform motion will add to the measured LOS velocity in ship coordinate system. Therefore, the first step in wind retrieval process is the removal of the along-beam platform velocity due to ship motion

15  $\vec{V}_{LOS\_ship}$ . It is noted that the wave-induced velocity perturbations would add to the ship's mean velocity when underway, which needs no correction independently in the correction procedure. During the experiment, the speed of the ship  $\vec{V}_{ship}$  is acquired by GNSS, and is recorded as the horizontal component  $\vec{V}_{ship\_horizontal}$  and vertical component  $\vec{V}_{ship\_vertical}$ , respectively thus the  $\vec{V}_{LOS\_ship}$  can be calculated



$$\vec{V}_{LOS\_ship} = \vec{r}_g \cdot \vec{V}_{ship} = \vec{V}_{ship\_horizontal} \cos(\psi - \varphi_g) \cos \theta_g + \vec{V}_{ship\_vertical} \sin \theta_g \quad (6)$$

The LOS velocity  $\vec{V}_{LOS}$  in Earth coordinate system is the vector sum of the LOS velocity measured by CDL in ship coordinate system  $\vec{V}_{LOS\_measure}$  and the  $\vec{V}_{LOS\_ship}$ , that is ,

$$\vec{V}_{LOS} = \vec{V}_{LOS\_measure} + \vec{V}_{LOS\_ship} \quad (7)$$

and

$$\vec{V}_{LOS} = \vec{r}_g \cdot \vec{V} + \vec{r}_g \cdot \vec{W} = u \cos \varphi_g \cos \theta_g + v \sin \varphi_g \cos \theta_g + w \sin \theta_g \quad (8)$$

where  $\vec{V} = [u, v, 0]$  and  $\vec{W} = [0, 0, w]$  are the horizontal and vertical component of the wind speed respectively,  $u$ ,  $v$  and  $w$  are the north-south, east-west and vertical velocity in Earth coordinate system, respectively.

Profiles of the wind vector can be retrieved by scanning the lidar beam or stepping the lidar beam through a sequence of different angles or perspectives (Reitebuch et al., 2001; Frehlich, 2001; Werner 2005). For the ground-based CDL, the profile of horizontal wind velocity can be retrieved using 4-Doppler Beam Swing (DBS) mode which is faster and simpler both in the hardware and in the data evaluation algorithm (Werner 2005; ~~Weikamp, 2006~~; Wang et al., 2010). Specifically, the wind vector components at target altitude can be derived by measuring the LOS wind velocities in four directions (normally east, west, south and north) under the assumption of cellular flow with little turbulence. But for the shipborne platform, the elevation  $\theta_g$  in four directions (north, south, west and east in ship coordination system) may have slightly difference (see Eq. (5)), thus a conversion of  $\vec{V}_{LOS}$  from real elevation  $\theta_g$  to the expected elevation  $\theta_0$  is firstly processed, that is,

$$\vec{V}'_{LOS} = \vec{V}_{LOS} \cos \theta_0 / \cos \theta_g \quad (9)$$

Furthermore, since the laser beam azimuth angle in Earth coordinate system need to be determined using Eq. (4), the conventional DBS formula where four measurement at azimuth-angle has an interval of  $90^\circ$  need to be modified. Then the  $u$ ,  $v$  can be calculated using modified 4-DBS formula

$$\begin{pmatrix} \cos \varphi_N - \cos \varphi_S & \sin \varphi_N - \sin \varphi_S \\ \cos \varphi_E - \cos \varphi_W & \sin \varphi_E - \sin \varphi_W \end{pmatrix} \begin{pmatrix} u \\ v \end{pmatrix} = \begin{pmatrix} (\vec{V}'_{LOS\_N} - \vec{V}'_{LOS\_S}) / \cos \theta_0 \\ (\vec{V}'_{LOS\_E} - \vec{V}'_{LOS\_W}) / \cos \theta_0 \end{pmatrix} \quad (10)$$

where the subscript  $N$ ,  $S$ ,  $E$ , and  $W$  represent the north, south, east and west in ship coordinate system, respectively.

For the case of vertical wind measurement, small deviation from vertical pointing due to ship motion induces a projection of the horizontal wind on the laser beam direction. To exactly correct this effect, estimation of the horizontal wind using Eq. (10)

are used, and then the vertical velocity  $w$  can be obtained using Eq. (8), where in this formula  $\vec{V}_{LOS}$  is the measurement in zenith stare mode. Figure 3 shows the flowchart of shipborne CDL data processing. Specifically, the LOS velocity and Signal



to Noise Ratio (SNR) can be firstly determined using lidar data and FFT analysis. It is noted that unlike the definition of SNR in previous studies (Banakh et al. 2013) where the SNR is defined as the ratio of the average heterodyne signal power to the averaged detector noise power in a 50-MHz bandwidth, the SNR in this paper is simpler and defined as the ratio of the peak value of FFT spectral signal in 50-MHz bandwidth in each range bin to the Root-Mean-Square-Error (RMSE) of background noise signal, also indicating the CDL detection capability, data accuracy and atmospheric tracer particle relative intensity. In this sense, the SNR threshold value in this paper is higher than the one in previous studies (Banakh et al. 2013; Achtert et al 2015) for the same signal power spectrum. After the data pre-processing including the quality control based on SNR threshold and averaging process, the attitude transformation is then used to obtain the azimuth and elevation in each LOS vector in Earth coordinate system. The LOS velocity detected by lidar is the atmosphere motion relative to ship coordinate system, thus the removal of the along-beam platform velocity due to ship motion is needed. Finally, the horizontal and vertical wind profiles can be retrieved using modified 4-DBS mode and zenith stare mode data correction, respectively.

### 3 Observation results and discussion

#### 3.1 Horizontal wind evaluation

The modified 4-DBS method for horizontal wind profile retrieval has been illustrated in Fig. 3. Two examples of the comparison between uncorrected and corrected horizontal wind profiles can be shown in Fig. 4 for anchored measurement and Fig. 5 for cruising observation, respectively, where the lidar results (black curves) averaged over at least 10 min after the launch of the radiosonde are compared with the radiosonde data (red curves). It is noted that the wind profile from lidar and radiosonde should be interpolated to the common height grid before comparison because of different spatial resolutions. The type of radiosonde is Model GTS1 digital radiosonde, the basic parameters of which are listed in Table 2 (Song et al., 2017).

Figure 4 shows the horizontal wind profile with anchored measurement (mean ship speed equals to  $0.27 \text{ ms}^{-1}$ ) during 15:52-16:02 Local Standard Time (LST) 9 May 2014 at  $37.00^\circ \text{ N}$ ,  $122.86^\circ \text{ E}$ . It can be seen that the wind is approximately southerly through the measurement altitude, but slightly southeasterly below 1.6 km, and then shifts to southwesterly above 1.6 km. The wind speed slightly increases below 0.2 km and gradually decreases with height till 1.6 km and then increases above. The blue bars represent the wind measurement fluctuation during analysed period, showing that the atmospheric condition is relative stable below 1.6 km whereas it is more changeable above 1.6 km where the wind direction has a continuous variation. The specific ship condition parameters are listed in Table 3. It can be seen that the mean pitch and roll are  $-0.17^\circ$  and  $0.63^\circ$  with standard deviation  $0.06^\circ$  and  $0.11^\circ$ , respectively, thus the swing of the ship is not obvious. Since lower SNR makes the data unavailable, data quality control based on SNR threshold is used to remove the spikes higher than 2.4 km. The RMSE in speed between lidar and radiosonde below 2 km are  $0.49 \text{ ms}^{-1}$  for the uncorrected measurement and  $0.45 \text{ ms}^{-1}$  for the corrected measurements, both showing consistent with the radiosonde wind speed. It is reasonable since the effect of ship motion speed on LOS velocity is less obvious in anchored measurement. Moreover, the variation of lidar elevation and azimuth





in Earth coordinate system is small, and in this case, for instance, when the lidar points to bow with elevation of  $60^\circ$  in ship coordinate system. If the ship's pitch, roll and heading are  $-0.17^\circ$ ,  $0.63^\circ$ ,  $5.28^\circ$ , respectively, according Eq. (4)-(5), the lidar azimuth and elevation in Earth coordinate are  $\varphi_s = 6.37^\circ$  and  $\theta_s = 59.82^\circ$ , respectively. Similarly, when the lidar points to starboard, stern and port, the corresponding azimuth are  $94.99^\circ$ ,  $184.18^\circ$  and  $275.58^\circ$ , and the elevation are  $59.37^\circ$ ,  $60.16^\circ$  and  $60.63^\circ$ , respectively, resulting in less difference of horizontal wind speed retrieved from the ship and Earth coordinate system. However, the RMSE in wind direction between lidar and radiosonde are  $84.43^\circ$  for uncorrected measurement and  $5.27^\circ$  for corrected measurement. The obvious difference of the wind direction results from two aspects. The first one is the definition in different coordinate systems, where the heading has an important effect on lidar azimuth. The second aspect is that because of the experimental field limitation, the direction of GNSS master antenna is perpendicular to the ship bow, meaning that the "real" heading is the recorded heading plus  $90^\circ$ , and this angle offset due to placement problem is fixed and calibrated using hard target detection before campaign. Generally, attitude correction is necessary, especially for the wind direction retrieval even though the ship is anchored with slight shake.

Figure 5 shows the results of the cruising observation from 07:44 to 07:54 LST on 13 May 2014 when the mean ship speed is  $4.84 \text{ ms}^{-1}$  with standard deviation  $0.03 \text{ ms}^{-1}$ . It can be seen that the wind is constantly southwesterly through the available measurement altitude, and there is a low-level-jet at around 0.3 km where the wind speed exceeds  $25 \text{ ms}^{-1}$ . What's more, the fluctuation in wind speed and direction above 1 km is more severe. The specific ship condition parameters are also listed in Table 3. It can be seen that the mean pitch and roll are  $-0.43^\circ$  and  $2.06^\circ$  with standard deviation  $0.05^\circ$  and  $0.87^\circ$ , respectively. Generally, the ship roll has a more effect on the lidar elevation when it points to the port or starboard, on the contrary, the lidar elevation in bow or stern direction is more sensitive to ship pitch. In this case, the lidar mean elevation in bow, starboard, stern and port direction after attitude transformation are  $59.51^\circ$ ,  $57.84^\circ$ ,  $60.30^\circ$  and  $62.49^\circ$ , respectively, and the mean heading is  $75.86^\circ$  with standard deviation  $1.22^\circ$  where the ship sails downwind. In this condition, the horizontal wind speed without motion correction will be underestimated compared with the radiosonde result. The RMSE in speed between lidar and radiosonde data below 1.0 km are  $4.42 \text{ ms}^{-1}$  for uncorrected measurement and  $0.88 \text{ ms}^{-1}$  for corrected measurements, and the corresponding RMSE in wind direction are  $48.71^\circ$  and  $9.52^\circ$ , respectively. Therefore, the attitude correction algorithm has obviously improved the wind profile result when the ship is in cruising observation. It can be seen that the discrepancies in wind profile above 1 km between the radiosonde and lidar measurement are significant due to the multipath effect at the ship platform and decrease in collocation of the measurement.

In order to assess the accuracy of the shipborne lidar wind measurement, the comparison of the lidar measurement and 11-radiosonde dataset during the experiment has been made. Figure 6 shows the scatter plot of wind speed and direction for radiosonde and lidar measurement based on modified 4-DBS solution. The red trend line plotted through these points represents





an ordinary linear least square regression for the data excluding  $|fdata - ydata| > 1.0 * SD$ , where  $fdata$  is the fitted value,  $ydata$  is the corresponding lidar result, and  $SD$  represents the standard deviation of  $ydata$ . The wind speed linear regression shows the correlation coefficient of 0.98 (the coefficient of determination of 0.96) and  $SD$  of  $0.75 \text{ ms}^{-1}$ . The wind direction linear regression shows the correlation coefficient of 0.99 (the coefficient of determination of 0.98) and  $SD$  of  $9.81^\circ$ . Both wind speed and direction show negligible biases, demonstrating the feasibility and reliability of the modified 4-DBS solution. Table 4 lists a height-resolved view (from 0.2 km to 1.6 km) of the linear fit parameters between lidar and radiosonde. The correlation coefficient  $R$  for wind direction is approximately 0.99 and almost constant with altitude up to 1.6 km. The correlation coefficient for wind speed is minimum at the lowest altitudes, and improves with height to values comparable to those for wind direction, the trends of which compare well with the results from Achtert et al (2015). On the one hand, the flow distortion around the ship would affect the low-level measurement from lidar and radiosonde with different effect on each due to different locations. On the other hand, the blind area of lidar is 150 m, meaning that too few data points are available below 200 m with effective comparison. An obvious feature in  $SD$ ,  $RMSE$ , normalized  $RMSE$  for wind speed and direction is found at the lowest levels where the discrepancies between lidar and radiosonde data are larger than the higher levels. The source of discrepancies is likely from flow distortion around the ship, which influences the lower-level measurement from lidar and radiosonde with different effects due to different locations. Furthermore,  $SD$ ,  $RMSE$ , normalized  $RMSE$  for wind speed and direction increase with altitude from 0.2 km, which are mainly caused by the drift of the radiosonde and increasing spatial separation between each other.

### 3.2 Vertical wind evaluation

The motion correction of vertical velocity, which is more obvious compared with the horizontal wind component, has been specifically described in Sect. 2. A typical measurement case study on 14 May 2014 is presented in Fig. 7. Figure 7a shows the whole series of time-height cross section of the SNR. It is noted that the data analysis below 0.15 km is not reliable because of the lidar blind area, and the data above 2.5 km is also removed since the SNR is less than its threshold value. In this paper, the SNR gradient method is used to retrieve the MABL height, and the height of the first strong negative gradient in SNR is regarded as the MABL height on the basis of the fact that the boundary layer has higher aerosol concentrations than the free troposphere above. The temporal and spatial variations of MABL height marked with black solid circles can be seen in Fig. 7a, where the marine stratocumulus structure is also presented at around 2.1 km during 07:33-08:40 LST. It can be seen that diurnal variation of MABL height is less obvious within 1.0 km - 1.5 km, consistent with the mixing layer height retrieved from the radiosonde potential temperature profile. Figure 7b shows the time series of ship heading, CDL laser beam azimuth and elevation, and horizontal wind direction at 0.4 km, respectively. The hemispherical scanner maintains the pointing of the lidar beam to zenith stare mode with an averaged elevation of  $88.6^\circ \pm 0.35^\circ$  because of the ship motion. During the zenith stare mode, the mean angle between ship heading and the laser azimuth is  $66^\circ$  with standard deviation of  $7^\circ$ , thus



the projection of ship velocity on vertical velocity is always positive, the results of which are shown in Fig. 8a. Furthermore, the estimation of the horizontal wind speed and direction (black line in Fig. 7b) from modified 4-DBS solution is used to remove the horizontal wind speed projection  $\vec{r}_g \cdot \vec{V}$  from the relative speed measured by CDL. In this case, the  $\vec{r}_g \cdot \vec{V}$  is positive and negative in downwind and headwind, respectively, causing the overestimate and underestimate of the vertical velocity, the effect of which is shown in Fig. 8b. The corrected vertical velocity wind speed is presented in Fig. 7c. The red and blue colour indicate positive (upward) and negative (downward) movement of the atmosphere parcels along the laser beam, respectively. It can be seen that the vertical velocity has a significant diurnal variation. Specifically, the downdraft dominants mixing layer in the morning and amounted to about  $0.5 \text{ ms}^{-1}$ , and small-scale convective activity can be observed at the top of mixing layer. As the solar radiation strengthens, the atmospheric convection becomes more active and extends to the whole mixing layer, the strengths of updrafts and downdrafts are weakly stronger than before and the atmospheric vertical alternation becomes more frequent. The mixing layer recovers to descending motions with a continuous and long period after 13:11 LST. The difference between the corrected and uncorrected vertical velocity can be shown in Fig. 8c, obviously showing the temporal and spatial variation of the contribution of ship motion and horizontal wind on vertical velocity.

### 3.3 Measurement uncertainty and error analysis

Error analysis is useful in assessing the accuracy and precision of the lidar wind measurements (Wang et al., 2010). They also shed light on the potential improvements of this CDL. According to the definition of error for measurement of a random wind field, the measured velocity is represented as (Frehlich, 2001):

$$\hat{V} = V_{truth} + e_v + bias_v \quad (11)$$

where  $V_{truth}$  is the desired or true wind measurement,  $e_v$  is the random error with zero mean, representing the precision of wind measurements, and  $bias_v$  is the systematic error, representing the accuracy of the wind measurements.

As for radial velocity, for instance, the north radial velocity  $\hat{V}_{LOS\_N}$  with azimuth angle  $\varphi_N$  and elevation angle  $\theta_N$ , the measurement can be represented as:

$$\hat{V}_{LOS\_N} = c_1 \bar{u} + c_2 \bar{v} + c_3 \bar{w} + e_N + bias_N \quad (12)$$

where  $\bar{h} = [\bar{u}, \bar{v}]$  and  $\bar{w}$  are the spatially averaged horizontal and vertical velocity, respectively,  $c_1 = \cos \varphi_N \cos \theta_N$ ,  $c_2 = \sin \varphi_N \cos \theta_N$ ,  $c_3 = \sin \theta_N$ ,  $e_N$  and  $bias_N$  are the random error and bias of the north radial velocity measurements, respectively.



For shipborne-based measurement, the ship platform velocity  $\vec{V}_{ship}$  produces a large contribution  $\vec{V}_{LOS\_ship}$  to the total radial velocity (see Eq. (6)). The bias in the radial velocity measurement comes from errors in the knowledge of  $\vec{V}_{ship\_horizontal}$ ,  $\vec{V}_{ship\_vertical}$ ,  $\psi_N$ ,  $\varphi_N$ ,  $\theta_N$ ,

$$\begin{aligned} bias_{LOS\_N} = & \Delta\vec{V}_{ship\_horizontal} \cos(\psi_N - \varphi_N) \cos\theta_N + \Delta\vec{V}_{ship\_vertical} \sin\theta_N - \\ & \Delta\psi_N \vec{V}_{ship\_horizontal} \cos\theta_N \sin(\psi_N - \varphi_N) + \Delta\varphi_N \vec{V}_{ship\_horizontal} \cos\theta_N \sin(\psi_N - \varphi_N) \\ & + \Delta\theta_N (\vec{V}_{ship\_vertical} \cos\theta_N - \vec{V}_{ship\_horizontal} \cos(\psi_N - \varphi_N) \sin\theta_N) \end{aligned} \quad (13)$$

where  $\Delta\vec{V}_{ship\_horizontal}$ ,  $\Delta\vec{V}_{ship\_vertical}$ ,  $\Delta\psi_N$  are the errors in the determination of the ship speed and direction, and equal to 0.1 ms<sup>-1</sup>, 0.1 ms<sup>-1</sup>, 0.1°, respectively.  $\Delta\theta_N$ ,  $\Delta\varphi_N$  are the pointing angle knowledge errors of the north direction lidar beam. In this case,  $\Delta\varphi$  and  $\Delta\theta$  are related to the servo system, and the scanner pointing accuracy is 0.1°, thus  $\Delta\varphi = \Delta\theta = 0.1^\circ$  in all directions.

Similarly, to derive the  $\vec{V}_{LOS}$  bias, we take the derivatives of Eq. (9)

$$bias_{LOS\_N} = bias_{LOS\_N} \cos\theta_0 / \cos\theta_N + \Delta\theta_N \vec{V}_{LOS\_N} \cos\theta_0 \sin\theta / \cos^2\theta_N \quad (14)$$

Estimation for the horizontal velocity are produced by solving Eq. (10) assuming that the wind field has a constant horizontal and vertical velocity, that is,

$$u = \frac{a_4 b_1 - a_2 b_2}{a_1 a_4 - a_2 a_3} \quad (15)$$

$$v = \frac{a_1 b_2 - a_3 b_1}{a_1 a_4 - a_2 a_3} \quad (16)$$

where  $a_1 = \cos\varphi_N - \cos\varphi_S$ ,  $a_2 = \sin\varphi_N - \sin\varphi_S$ ,  $a_3 = \cos\varphi_E - \cos\varphi_W$ ,  $a_4 = \sin\varphi_E - \sin\varphi_W$ ,  $b_1 = (\vec{V}_{LOS\_N} - \vec{V}_{LOS\_S}) / \cos\theta_0$ ,  $b_2 = (\vec{V}_{LOS\_E} - \vec{V}_{LOS\_W}) / \cos\theta_0$ .

Since the error in the lidar pointing angle should be very small, one can assume perfect knowledge of the coefficient  $a_i$  (Frehlich, 2001), so the biases of  $u$  and  $v$  from the radial velocity estimation can be described:

$$bias_u = \frac{a_4 bias_{b_1} - a_2 bias_{b_2}}{a_1 a_4 - a_2 a_3} \quad (17)$$



$$bias_v = \frac{a_1 bias_{b_2} - a_3 bias_{b_1}}{a_1 a_4 - a_2 a_3} \quad (18)$$

It can be seen that the dominant source of bias of the horizontal velocity estimates come from the biases of the radial velocity estimates ( $bias_N$ ,  $bias_S$ ,  $bias_E$  and  $bias_W$ ), which are determined by the error in the ship velocity and lidar pointing errors.

Following the approach of Frehlich (Frehlich, 2001; Frehlich, 1996), a method based on the frequency spectrum of the retrieved velocity has been used to determine the random error of horizontal and vertical wind measurements, which assumes that the estimation error is uncorrelated with the random variations in the velocity field and aerosol backscatter.

Figure 9 shows the error analysis of horizontal wind during 15:52-16:02 LST 09 May 2014. In this case, a 50 % window overlap factor, a Hamming window and a zero-padding of the missing values were applied to each window for each spectrum calculation (Frehlich, 2001; Chouza et al., 2016). The resulting spectrum shows that the frequencies higher than 0.2 Hz tend to be a constant value, and the high-frequency region represents the spectrum of the random noise. The observed SNR is illustrated in the Fig. 9a, and there is an aerosol layer at around 1.5 km, consistent with the higher value in SNR. The random errors from the standard deviation of the random noise signal, shown in Fig. 9b, are less than  $0.1 \text{ ms}^{-1}$  below 1 km with  $\text{SNR} < 8 \text{ dB}$ , and a peak value appears at around 1.3 km and decreases with altitude till at around 1.5 km. Then the random errors increase with altitude as the SNR decrease, and reach about  $1.2 \text{ ms}^{-1}$  at 2.3 km. It is clear that the random error is mainly determined by the SNR. Figure 9c shows the  $bias_u$ ,  $bias_v$  and corresponding bias of horizontal wind velocity  $bias_h$ . The  $bias_h$  is less than  $0.02 \text{ ms}^{-1}$  below 2.5 km, which is negligible and consistent with the result shown in section 4.1. According to Eq. (13)-(18), the dominant source of bias of horizontal wind velocity is mainly from the ship velocity and lidar pointing errors in different direction. In this case, the  $\vec{V}_{ship\_horizontal}$  has the most effect on the bias of the radial velocity. The bias of horizontal wind speed is typically less than the random error which is determined from the frequency spectrum of the retrieved horizontal velocity

The observed random error of the vertical velocity as a function of SNR is presented in Fig. 10, which is retrieved from the frequency spectrum of the retrieved vertical velocity during 07:33 to 15:29 LST 14 May 2014. It can be seen that in the high SNR region above 8 dB, a constant random error range between  $0.03$  and  $0.15 \text{ ms}^{-1}$  is found because of the effect of the speckle-induced phase noise (Achtert et al., 2015), which is much smaller than the discrepancy between the mean wind speed derived from lidar and radiosonde of  $0.75 \text{ ms}^{-1}$  (see Sect. 3.1). At reduced values of the SNR, the errors increase as a result of increasing signal noise, rising to approximately  $4 \text{ ms}^{-1}$  at an  $\text{SNR} = 0 \text{ dB}$ . It is confirmed that the choice of a conservative SNR threshold of 8 dB is robust for data quality control process.



#### 4 Summary

Shipborne wind observation by the CDL during the 2014 Yellow Sea campaign has been presented to study the structure of the MABL. The algorithm-based attitude and velocity correction methods greatly relax the requirements for mechanical stability and compensation mechanisms. The attitude correction system of CDL consists of GNSS and inertial navigation system to directly measure the speed and the attitude of the ship. According to the transformation matrix from the product of roll, pitch and heading rotation matrix, the azimuth and elevation of the LOS velocity in the Earth coordinate system can be firstly determined. Then the removal of the along-beam platform velocity due to ship motion is needed to obtain the “real” LOS velocity in the Earth coordinate system. The horizontal wind profiles can be retrieved by a modified 4-DBS method. For the case of vertical velocity, small deviations from vertical pointing due to ship motion induces a projection of the horizontal wind on the LOS vector, thus estimation of the horizontal wind speed contribution are used to correct the vertical velocity.

The comparison of the CDL to radiosonde shows that attitude correction is essential for the wind retrieval in cruising measurement. The correlation coefficients of wind speed and direction are 0.98, 0.99, respectively, both of which show negligible bias and demonstrate the feasibility and reliability of the modified 4-DBS method. A case study of 8-h time series observation on 14 May 2014 is presented to compare uncorrected and corrected vertical velocity, additionally showing the specific temporal and spatial variation of the contributions of ship motion and horizontal wind on vertical velocity.

The bias of horizontal wind velocity was estimated using error propagation analysis and concluded that the dominant source comes from the radial velocity estimates, which are determined by the error in the ship velocity and lidar pointing errors. The random error was estimated based on the frequency spectrum of the retrieved velocity. Based on one measurement case, the random error of horizontal wind velocity was between  $0.03 \text{ ms}^{-1}$  and  $1.2 \text{ ms}^{-1}$  in different heights, and it is mainly determined by the SNR, while the bias was less than  $0.02 \text{ ms}^{-1}$ , which is negligible and consistent with the result of comparison between lidar and radiosonde data. The fundamental random error of the lidar vertical wind was found to be in the range of 0.03 to  $0.15 \text{ ms}^{-1}$  for SNR above 8 dB, which is much smaller than the discrepancy between the mean wind speed derived from lidar and radiosonde of  $0.75 \text{ ms}^{-1}$ . The choice of a conservative SNR threshold of 8 dB was also confirmed by the error analysis results of vertical velocity. Overall, combining a CDL with attitude correction system and accurate motion correction process as presented here forms a reliable and autonomous set-up that could be placed on mobile platform to provide measurement for MABL thermodynamic process, air-sea interaction and so forth, providing much more detailed, higher spatial and temporal resolution view of MABL process.



## Acknowledgements

This work was partly supported by the National High Technology Research and Development Program of China under grant 2014AA09A511, the National Natural Science Foundation of China under grant 41471309 and 41375016, and the National Key Research and Development Program of China under grant 2016YFC1400904.

## 5 References

- Achtert, P., Brooks, I., Brooks, B., Moat, B., Prytherch, J., Persson, P., and Tjernström, M.: Measurement of wind profiles by motion-stabilised ship-borne Doppler lidar, *Atmos. Meas. Tech.*, 8, 4993-5007, 2015.
- Axford, D.: On the accuracy of wind measurements using an inertial platform in an aircraft, and an example of a measurement of the vertical mesostructure of the atmosphere, *J. Appl. Meteorol.*, 7, 645-666, 1968.
- 10 Anctil, F., Donelan, M. A., Drennan, W. M., and Graber, H. C.: Eddy-correlation measurements of air-sea fluxes from a discus buoy, *J. Atmos. Oceanic. Technol.*, 11, 1144-1150, 1994.
- Banakh, V., and Smalikho, I.: Coherent Doppler wind lidars in a turbulent atmosphere: Artech House, 2013.
- Banta, R. M., Pichugina, Y. L., and Brewer, W. A.: Turbulent velocity-variance profiles in the stable boundary layer generated by a nocturnal low-level jet, *J. Atmos. Sci.*, 63, 2700-2719, 2006.
- 15 Bradley, E. F., Coppin, P., and Godfrey, J.: Measurements of sensible and latent heat flux in the western equatorial Pacific Ocean, *J. Geophys. Res.: Oceans*, 96, 3375-3389, 1991.
- Cheong, B., Palmer, R., Yu, T., Yang, K., Hoffman, M., Frasier, S., and Lopez-Dekker, F.: Effects of wind field inhomogeneities on Doppler beam swinging revealed by an imaging radar, *J. Atmos. Oceanic. Technol.*, 25, 1414-1422, 2008.
- 20 Chouza, F., Reitebuch, O., Jähn, M., Rahm, S., and Weinzierl, B.: Vertical wind retrieved by airborne lidar and analysis of island induced gravity waves in combination with numerical models and in situ particle measurements, *Atmos. Chem. Phys.*, 16, 2016.
- Dunkel, M., Hasse, L., Krügermeyer, L., Schriever, D., and Wucknitz, J.: Turbulent fluxes of momentum, heat and water vapor in the atmospheric surface layer at sea during ATEX, *Boundary-Layer Meteorol.*, 6, 81-106, 1974.
- 25 Edson, J. B., Hinton, A. A., Prada, K. E., Hare, J. E., and Fairall, C. W.: Direct covariance flux estimates from mobile platforms at sea\*, *J. Atmos. Oceanic. Technol.*, 15, 547-562, 1998.
- Fairall, C., Hare, J., Edson, J., and McGillis, W.: Parameterization and micrometeorological measurement of air-sea gas transfer, *Boundary-Layer Meteorol.*, 96, 63-106, 2000.



- Frehlich, R.: Simulation of coherent Doppler lidar performance in the weak-signal regime, *J. Atmos. Oceanic. Technol.*, 13, 646-658, 1996.
- Frehlich, R.: Errors for space-based Doppler lidar wind measurements: Definition, performance, and verification, *J. Atmos. Oceanic. Technol.*, 18, 1749-1772, 2001.
- 5 Fujitani, T.: Method of turbulent flux measurement on a ship by using a stable platform system, *Papers in Meteorol. Geophys.*, 36, 157-170, 1985.
- Fujitani, T.: Turbulent transport mechanism in the surface layer over the tropical ocean, *J. Meteorol. Soc. Jpn.*, 70, 795-811, 1992.
- Hawley, J. G., Targ, R., Henderson, S. W., Hale, C. P., Kavaya, M. J., and Moerder, D.: Coherent launch-site atmospheric  
10 wind sounder: theory and experiment, *Appl. Opt.*, 32, 4557-4568, 1993.
- Hill, R. J.: Motion compensation for shipborne radars and lidars, US Department of Commerce, National Oceanic and Atmospheric Administration, Office of Oceanic and Atmospheric Research, Earth System Research Laboratory, Physical Sciences Division, 2005.
- Hill, R. J., Brewer, W. A., and Tucker, S. C.: Platform-motion correction of velocity measured by Doppler lidar, *J. Atmos.*  
15 *Oceanic. Technol.*, 25, 1369-1382, 2008.
- Lenschow, D., Pearson, R., and Stankov, B.: Estimating the ozone budget in the boundary layer by use of aircraft measurements of ozone eddy flux and mean concentration, *J. Geophys. Res.: Oceans.*, 86, 7291-7297, 1981.
- Lenschow, D.: Aircraft measurements in the boundary layer, *Probing. Atmos. Boundary. Layer.*, 39-55, 1986.
- Liu, B.-Y., Liu, Z.-S., Song, X.-Q., Wu, S.-H., Bi, D.-C., Wang, X.-T., Yin, Q.-W., and Reitebuch, O.: Modifications and  
20 Moving Measurements of Mobile Doppler LIDAR, ESA Special Publication, 2010, 30.
- Miller, S. D., Hristov, T. S., Edson, J. B., and Friehe, C. A.: Platform motion effects on measurements of turbulence and air-sea exchange over the open ocean, *J. Atmos. Oceanic. Technol.*, 25, 1683-1694, 2008.
- Mitsuta, Y., and Fujitani, T.: Direct measurement of turbulent fluxes on a cruising ship, *Boundary-Layer Meteorol.*, 6, 203-217, 1974.
- 25 Pichugina, Y. L., Banta, R. M., Brewer, W. A., Sandberg, S. P., and Hardesty, R. M.: Doppler lidar-based wind-profile measurement system for offshore wind-energy and other marine boundary layer applications, *J. Appl. Meteorol. Clim.*, 51, 327-349, 2012.





- Reitebuch, O., Werner, C., Leike, I., Delville, P., Flamant, P. H., Cress, A., and Engelbart, D.: Experimental Validation of Wind Profiling Performed by the Airborne 10- $\mu$ -m Heterodyne Doppler Lidar WIND, *J. Atmos. Oceanic. Technol.*, 18, 1331-1344, 2001.
- Rocers, D. P., Johnson, D. W., and Friehe, C. A.: The stable internal boundary layer over a coastal sea. Part I: Airborne measurements of the mean and turbulence structure, *J. Atmos. Sci.*, 52, 667-683, 1995.
- Schulz, E., Sanderson, B., and Bradley, E. F.: Motion correction for shipborne turbulence sensors, *J. Atmos. Oceanic. Technol.*, 22, 55-69, 2005.
- Shao, Y.: Correction of Turbulent Wind Measurements Contaminated by Irregular Motion of a Ship, TOGA-COARE Project, CSIRO Center for Environmental Mechanics, Canberra, Australia, Technical Report, 1995.
- Song, X., Friehe, C. A., and Hu, D.: Ship-board measurements and estimations of air-sea fluxes in the western tropical Pacific during TOGA COARE, *Boundary-Layer Meteorol.*, 81, 373-397, 1996.
- Song, X., Zhai, X., Liu, L., and Wu, S.: Lidar and Ceilometer Observations and Comparisons of Atmospheric Cloud Structure at Nagqu of Tibetan Plateau in 2014 Summer, *Atmosphere*, 8(1), 9, 2017.
- Tsukamoto, O.; Ishida, H.: Turbulent flux measurements and energy budget analysis over the equatorial Pacific during TOGA-COARE IOP. *J. Meteorol. Soc. Jpn.*, 73, 557-568, 1995.
- Tucker, S. C., Senff, C. J., Weickmann, A. M., Brewer, W. A., Banta, R. M., Sandberg, S. P., Law, D. C., and Hardesty, R. M.: Doppler lidar estimation of mixing height using turbulence, shear, and aerosol profiles, *J. Atmos. Oceanic. Technol.*, 26, 673-688, 2009.
- Wang, Z., Liu, Z., Liu, L., Wu, S., Liu, B., Li, Z., and Chu, X.: Iodine-filter-based mobile Doppler lidar to make continuous and full-azimuth-scanned wind measurements: data acquisition and analysis system, data retrieval methods, and error analysis, *Appl. Opt.*, 49, 6960-6978, 2010.
- Weitkamp, C.: Lidar: range-resolved optical remote sensing of the atmosphere, Springer Science & Business, 2006.
- Werner, C.: Doppler Wind Lidar, edited by: Weitkamp, Springer, New York, 325–353, 2005.
- Wolfe, D., Brewer, W., Tucker, S., White, A., White, D., Welsh, D., Ruffieux, D., Fairall, C., Ratterree, M., and Intrieri, J.: Shipboard multisensor merged wind profiles from the New England Air Quality Study 2004, *J. Geophys. Res.: Atmos.* 112, 2007.
- Wu, S., Liu, B., Liu, J., Zhai, X., Feng, C., Wang, G., Zhang, H., Yin, J., Wang, X., Li, R., and Gallacher, D.: Wind turbine wake visualization and characteristics analysis by Doppler lidar, *Opt. Express*, 24(10), A762-A780, 2016.



Wulfmeyer, V., and Janjic, T.: Twenty-four-hour observations of the marine boundary layer using shipborne NOAA high-resolution Doppler lidar, J. Appl. Meteorol., 44, 1723-1744, 2005.

Zhai, X., Wu, S., and Liu, B.: Doppler lidar investigation of wind turbine wake characteristics and atmospheric turbulence under different surface roughness, Opt. Express, 25, A515-A529 2017.

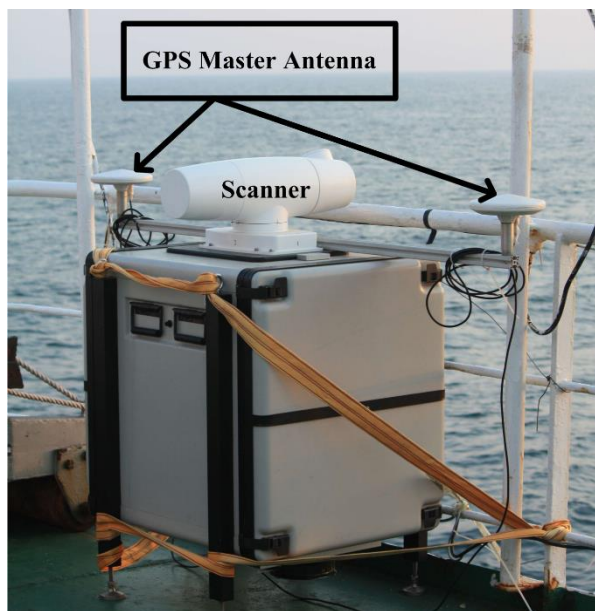


Figure 1: The Coherent Doppler Lidar setup on Dongfanghong-2 research vessel.

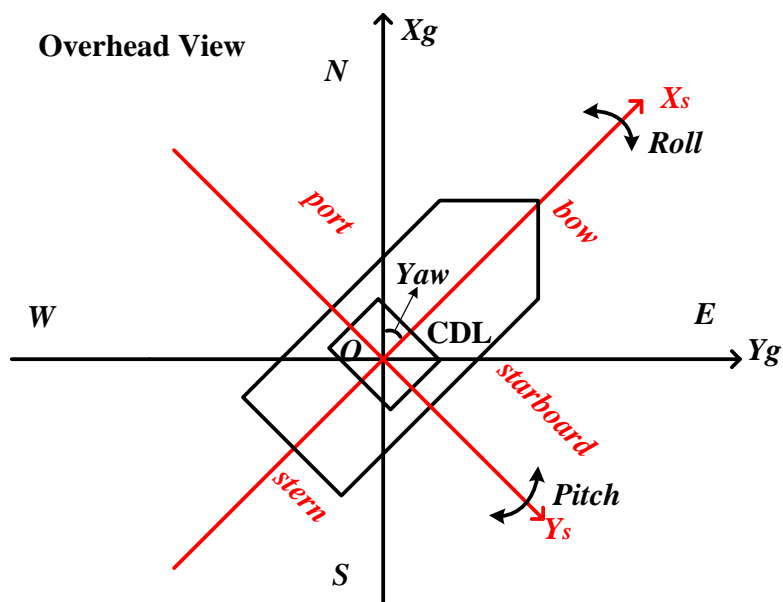
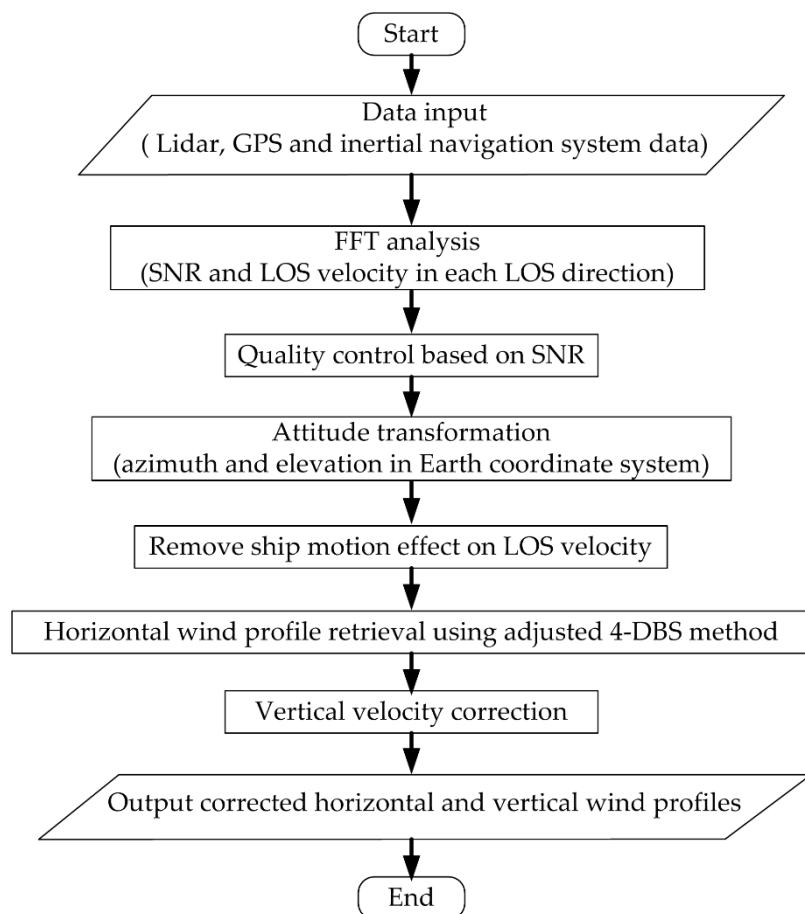
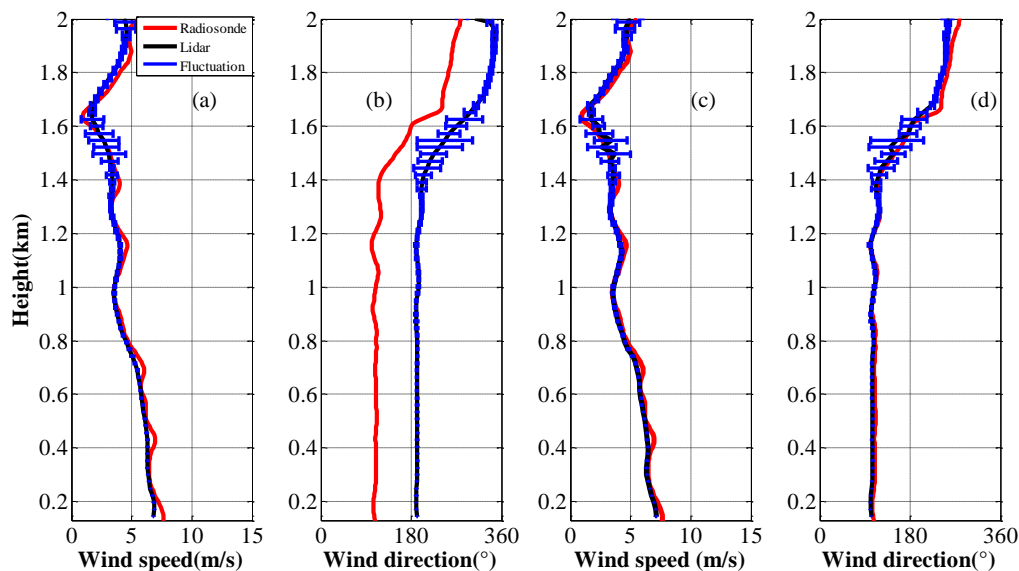


Figure 2: The overhead view of ship and Earth coordinate system.



**Figure 3: Flow chart of ship motion correction algorithm based on CDL.**



**Figure 4: Anchored observation: (a) (c) wind speed and (b) (d) wind direction measured by CDL (blue line) before and after attitude correction, respectively. The simultaneous radiosonde data is shown in red line. The blue bars represent the sampling fluctuations from 15:52 to 16:02 LST, 09 May, 2014.**

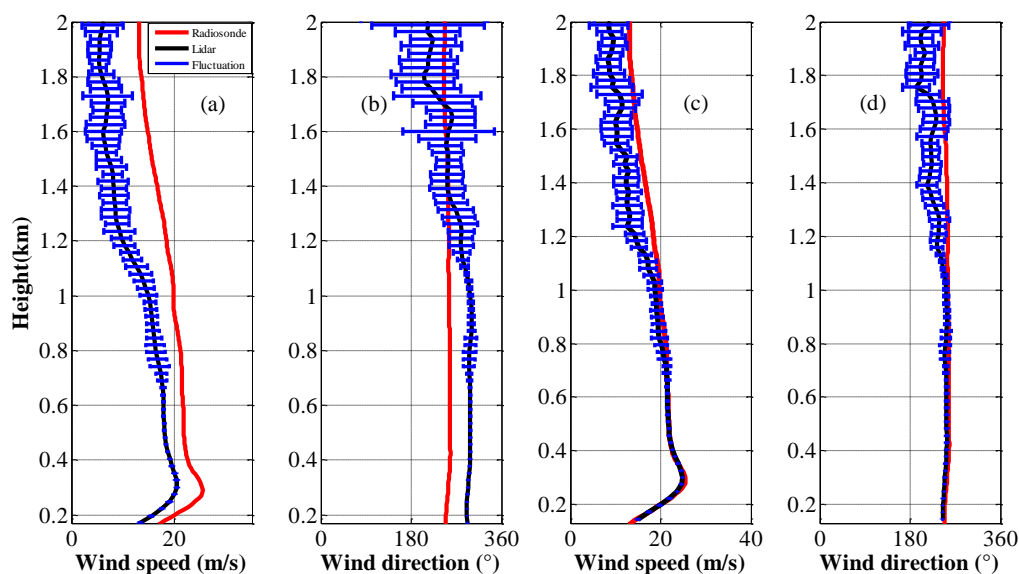


**Figure 5: As Fig. 4, but for 07:44 to 07:54 LST 13 May, 2014 in cruising observation.**

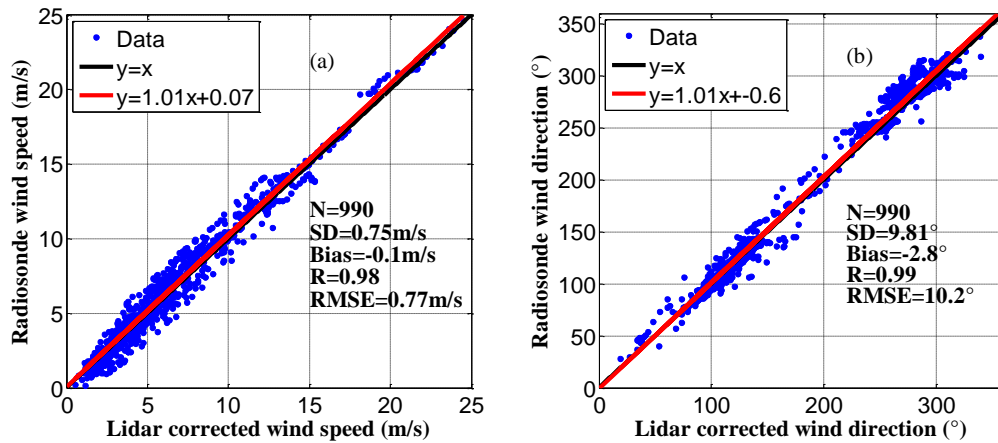


Figure 6: Comparison of (a) wind speed and (b) wind direction between CDL and radiosonde data from 09 May 2014 to 19 May 2014. The number of points (N), standard deviation (SD), bias, correlation coefficient (R), and root-mean-square-error (RMSE) are also listed.

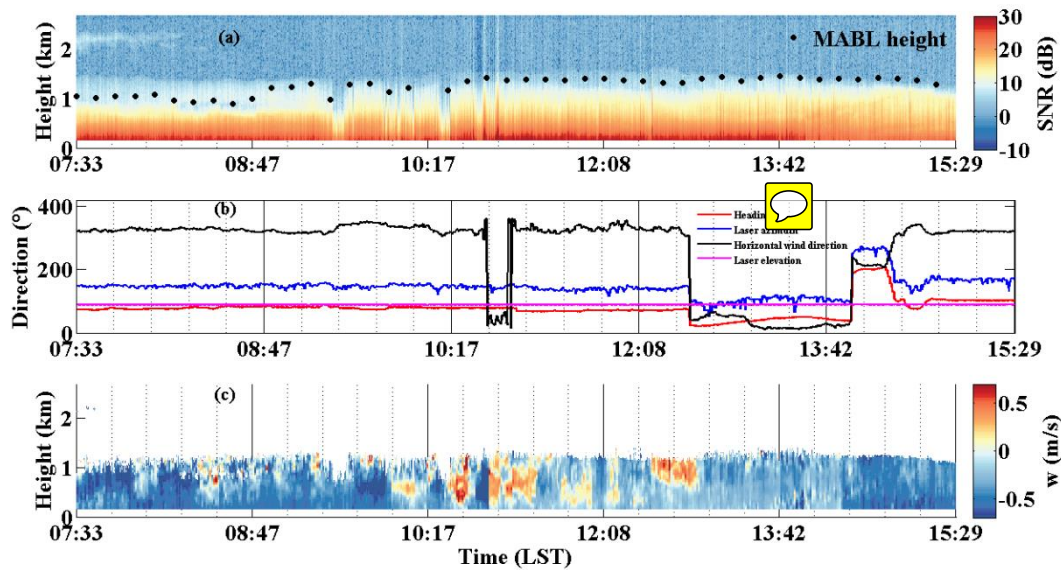
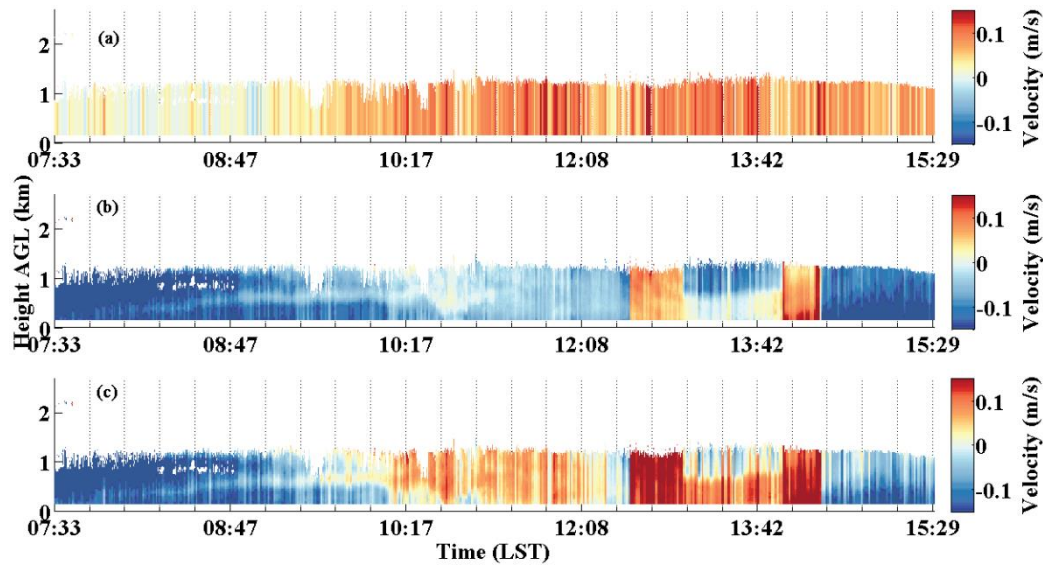


Figure 7: Example measurement from 07:33 to 15:29 LST 14 May 2014: (a) Time-Height-Intensity of SNR and retrieved MABL height using SNR gradient method (black solid circles). (b) time series of ship heading, CDL laser beam azimuth and elevation in the Earth coordinate system, and horizontal wind direction at 0.4 km. (c) Time-Height-Intensity of vertical velocity after attitude correction.



**Figure 8: Vertical velocity correction analysis: (a) projection of ship velocity on vertical velocity:  $\vec{V}_{LOS\_ship}$  (b) the effect of horizontal wind on vertical velocity:  $-\vec{r}_g \cdot \vec{V}$  (c) difference between vertical velocity after attitude correction and vertical velocity before attitude correction.**

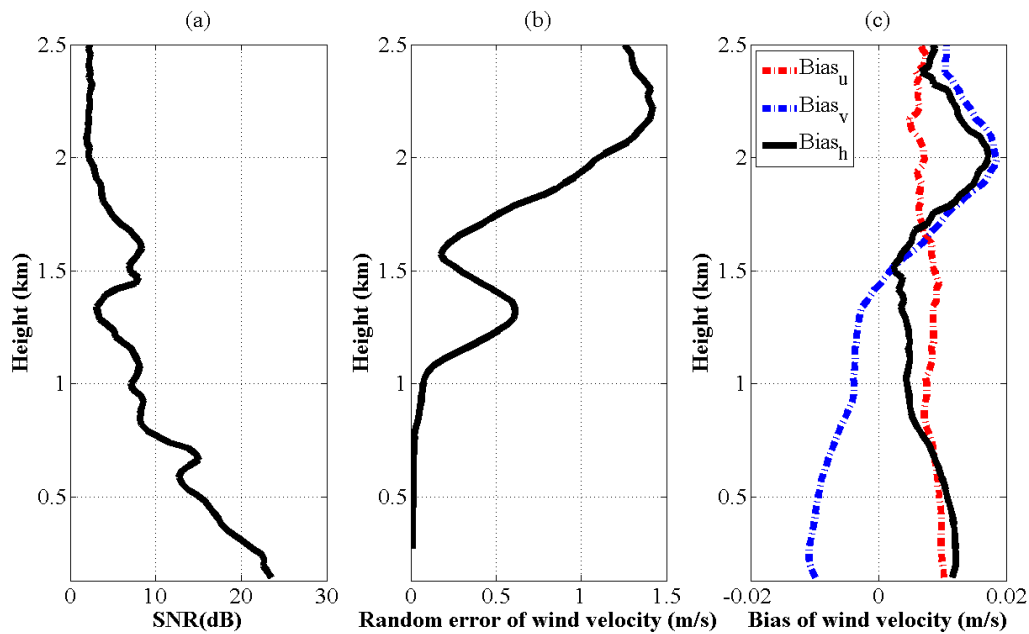




Figure 9: The averaged profile of (a) SNR (b) Random error of horizontal wind velocity (c) bias of horizontal wind north-south component (u), east-west component (v) and horizontal wind velocity measured by CDL from 15:52 to 16:02 LST, 09 May, 2014.

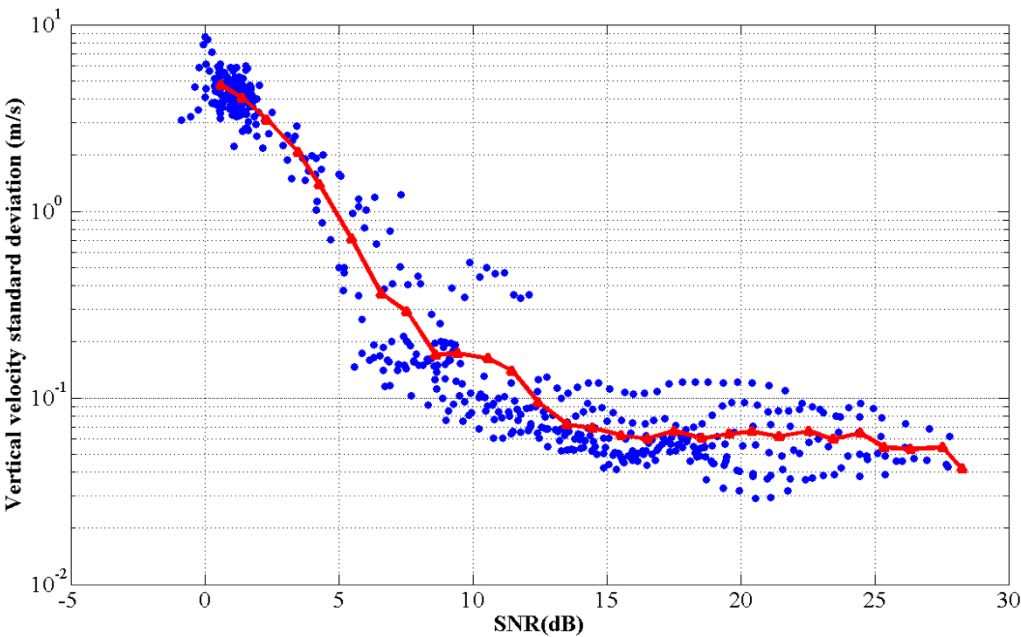



Figure 10: Random error of the CDL vertical velocity from 07:33 to 15:29 LST 14 May 2014 in all height range, which is determined from the frequency spectrum of the retrieved vertical velocity. The averaged random error per SNR bin is shown in red-triangle line.

Table 1: Component Parameters of the CDL system


Qualification	Specification
Wavelength	1.55 $\mu\text{m}$
Pulse repetition rate	10 kHz
Pulse width	100 ns - 400 ns
Pulse energy	150 $\mu\text{J}$
Measurement range	80 m - 4000 m (6000 m maximum)
Range resolution	15 m - 60 m





Speed measurement uncertainty	$\leq 0.1 \text{ ms}^{-1}$
Power dissipation 	$< 300 \text{ W}$
weight	$\sim 75 \text{ kg}$


**Table 2: Component parameters of the GTS1 radiosonde**

Meteorological Sensor	Specification	Technical Parameter
	Range	-90 - 50 °C  C (-80 - 50 °C) 0.3 °C (-90 - -80 °C)
	Resolution	0.1 °C
	Range	0% RH - 100% RH 5% RH (T ≥ 25 °C) 10% RH (T ≤ 25 °C)
	Resolution	1% RH
	Range	1060 hPa - 5 hPa 2 hPa (1050 hPa - 500 hPa) 1 hPa (500 hPa - 5 hPa)
	Resolution	0.1 hPa

**Table 3: Ship motion parameters during anchored and cruising observations, respectively.**

Date period	pitch	Roll	heading	Ship speed
2014.05.09 15:52-16:02	$-0.17^\circ \pm 0.06^\circ$	$0.63^\circ \pm 0.11^\circ$	$5.28^\circ \pm 1.22^\circ$	$0.27 \text{ ms}^{-1} \pm 0.01 \text{ ms}^{-1}$
2014.05.13 07:44-07:54	$-0.43^\circ \pm 0.05^\circ$	$2.06^\circ \pm 0.87^\circ$	$75.86^\circ \pm 1.22^\circ$	$4.84 \text{ ms}^{-1} \pm 0.03 \text{ ms}^{-1}$



**Table 4: Statistics of the comparison between CDL and radiosonde at heights of 0.2, 0.4, 0.8, 1.2 and 1.6 km. Normalized RMSE is defined as RMSE divided by the maximum range of the measured values (maximum-minimum).** 

	Wind speed					Wind direction				
Height (km)	0.2	0.4	0.8	1.2	1.6	0.2	0.4	0.8	1.2	1.6
Number points	84	104	104	87	65	89	93	96	90	88
SD ( $\text{ms}^{-1}$ )/( $^{\circ}$ )	0.83	0.49	0.46	0.67	0.77	9.77	6.71	8.23	9.39	10.8
Bias ( $\text{ms}^{-1}$ )/( $^{\circ}$ )	0	-0.1	-0.3	0.26	-0.5	-3.4	-2.7	0	-0.1	-6.3
R	0.97	0.99	0.99	0.98	0.98	0.99	0.99	0.99	0.99	0.98
RMSE ( $\text{ms}^{-1}$ )/( $^{\circ}$ )	0.83	0.50	0.59	0.72	0.94	10.3	7.22	8.18	9.34	12.5
Normalized RMSE (%)	4.55	2.31	3.32	5.93	7.44	4.27	3.17	3.18	3.4	6.81
Slope	1	0.99	1.04	1.09	1.10	0.99	1.01	1.01	1.09	1.10
Intercept ( $\text{ms}^{-1}$ )/( $^{\circ}$ )	0	0.2	0.01	-0.9	0.03	4.23	0.77	-1.7	-4.9	5.1